The Astrophysical Journal, 859:120 (6pp), 2018 June 1 https://doi.org/10.3847/1538-4357/aabee2

In Situ Observations of Harmonic Alfvén Waves and Associated Heavy Ion Heating

Huayue Chen, Xinliang Gao, Quanming Lu, and Shui Wang
CAS Key Laboratory of Geoscience Environment, School of Earth and Space Sciences, University of Science and Technology of China, Hefei, 230026, People's Republic of China; gaoxl@mail.ustc.edu.cn, qmlu@ustc.edu.cn
Received 2018 January 10; revised 2018 April 10; accepted 2018 April 15; published 2018 May 30

Abstract

Resonant ion heating by high-frequency Alfvén waves has long been believed to be the primary dissipation mechanism for solar coronal heating, and these high-frequency Alfvén waves are considered to be generated via cascade from low-frequency Alfvén waves. In this study, we report an unusual harmonic Alfvén event from in situ observations by the *Van Allen Probes* in the magnetosphere, having an environment similar to that in the solar corona. The harmonic Alfvén waves, which propagate almost along the wave vector of the fundamental waves, are considered to be generated due to the interaction between quasi-parallel Alfvén waves and plasma density fluctuations with almost identical frequency. These high-frequency harmonic Alfvén waves can then cyclotron resonantly heat the heavy ions. Our observations provide an important insight into solar corona heating by Alfvén waves.

Key words: methods: observational – Sun: atmosphere – waves

1. Introduction

The temperature of the solar corona can be up to hundreds of times that of the underlying photosphere. Using remote-sensing observations, the Ultraviolet Coronagraph and Spectrograph on the *Solar and Heliospheric Observatory* spacecraft have further shown that heavy ions in coronal holes are much hotter than protons, and their velocity distributions exhibit a strong anisotropy with the perpendicular temperature much larger than the parallel temperature (Kohl et al. 1997, 1998; Li et al. 1998; Cranmer et al. 1999). To resolve this long-standing mystery, an efficient dissipation process is obligatory to heat the solar corona.

Among the possible heating scenarios of the solar corona, Alfvén waves, through cyclotron resonant interactions with particles, emerge as the most promising candidates. Plenty of theoretical models based on resonant scattering of particles by Alfvén waves are proposed to explain the plasma heating of the solar corona (Tu & Marsch 1997; Hollweg 1999; Cranmer 2000; Isenberg et al. 2001). The resonant condition can be satisfied only when the wave frequency is comparable to the ion gyrofrequency, and the generation of high-frequency Alfvén waves via cascade becomes the critical point for coronal heating (Isenberg & Hollweg 1983; Tu 1987; Hollweg & Johnson 1988; Cranmer & van Ballegooijen 2003). However, theoretical studies have shown that the cascade of Alfvén waves preferentially occurs in the perpendicular direction (Sridhar & Goldreich 1994; Goldreich & Sridhar 1995; Quataert 1998; Vasquez et al. 2014), and the measurements of the parallel and perpendicular spectra of Alfvén waves down to the ion inertial scale near 1 au have indicated that this kind of cascade process occurs in the solar wind (Bale et al. 2005; Sahraoui et al. 2010; He et al. 2012; Podesta & TenBarge 2012). The perpendicular cascade of Alfvén waves would lead to the generation of kinetic Alfvén waves in the dissipation range, where the dissipation is dominated by electron Landau damping in the parallel direction (Leamon et al. 1999; Gary & Nishimura 2004; Howes et al. 2008). To date, there is still a lack of direct observations of Alfvénic cascade to high frequency. In this study, we report an unusual harmonic Alfvén event in the wave propagating direction from in situ observations by the *Van Allen Probes* in the magnetosphere. Here, the plasma beta is very low, which is similar to that in the solar corona, and the heavy ions are then preferentially heated in the perpendicular direction through cyclotron resonant scattering. Our observations provide an insight on how high-frequency Alfvén waves are generated in the solar corona.

The paper is organized as follows. In Section 2, we briefly describe the analysis of the *Van Allen Probes* data. Observational results including the dynamic spectrum of Alfvén event and the time history of ion flux are given in Section 3. Finally we summarize and further discuss the principal results of the present study in Section 4.

2. *Van Allen Probe* Data Analysis

The observations are from the *Van Allen Probes* mission, which has twin satellites (probes A and B) operating in a near-equatorial orbit with apogees of ~5.8 R_E (Kessel et al. 2012; Mauk et al. 2013). Both satellites are equipped with comprehensive suites for the monitoring of wave environment and radiation belt particles. The DC magnetic field vector information is provided by a triaxial fluxgate magnetometer (MAG) from the Electric and Magnetic Field Instrument Suite and Integrated Science (EMFISIS) on board both spacecraft with 64 samples s^{-1} (Kletzing et al. 2013). The 32 Hz three-axis electric field is measured by the Electric Field and Waves (EFW) instrument, which can also provide data on plasma density estimated from the spacecraft potential (Wygant et al. 2013). For waveform analysis, we first convert these triaxial magnetic and electric field data into magnetic field-aligned coordinates, following the method in Usanova et al. (2016). Then, a sliding window fast Fourier transform of 4096-points is utilized to calculate the corresponding power spectral density.

Here we perform the ion flux measured from the Helium, Oxygen, Proton, and Electron (HOPE) mass spectrometer (Funsten et al. 2013) and the Radiation Belt Storm Probes Ion Composition Experiment (RBSPICE) (Mitchell et al. 2013), all utilizing time-of-flight technology. HOPE can measure the

energy range of 1 eV–50 keV and distinguish three major ion species: H^+, He^+, and O^+, while RBSPICE can provide the flux measurements in relatively higher-energy channels of H^+ in 50–600 keV, He^+ in 65–520 keV, and O^+ in 140–1130 keV.

3. Observational Results

The Alfvén wave event is captured by *Van Allen Probe* B at $L \approx 4.0\,R_E$, magnetic local time ≈ 15 hr, and magnetic latitude $\approx -1.6^{\circ}$ during 04:40:00–04:52:00 UT, on 2013 October 9. Figure 1 illustrates an overview of this event, including (a)–(d) the dynamic spectrogram of fluctuating magnetic ($B_\perp$ and $B_{||}$) and electric ($E_\perp$ and $E_{||}$) fields, respectively, (e) "Pflag," representing the wave propagating direction, (f) the wave normal angle θ, and (g) the ellipticity ε. In all panels, the dotted and dashed lines in black or white represent the local helium gyrofrequency f_{He^+} and oxygen gyrofrequency f_{O^+}, respectively. In Figure 1(e), Pflag denotes the propagating direction of the waves, where Pflag $= 1$ means that the waves are propagating away from the magnetic equator, and propagating toward it when Pflag $= -1$ (Santolík et al. 2010). Both the wave normal angle θ and the ellipticity ε are calculated from the wave detection algorithm (Bortnik et al. 2007). In this algorithm, $\varepsilon = -1$ or 1 means that the waves have left-hand or right-hand polarization, while they have linear polarization when $\varepsilon = 0$. We find that the amplitude of the Alfvén waves is enhanced rapidly around 04:42:00 UT, and the fluctuations are concentrated mainly in the perpendicular direction. The waves exhibit a spectral structure with several bands, and detailed analysis shows that it is composed of a fundamental wave and several of its harmonics. The fundamental wave has a frequency between the oxygen and helium gyrofrequency. At almost every time, Pflag is mixed with -1 and 1, which means that the waves are counter-propagating modes quasi-parallel to the background magnetic field with the wave normal angle $\theta < 20^{\circ}$. These waves are located in their source region, where they are just excited. $\varepsilon \approx 0$ represents that these waves have nearly linear polarization. Besides the perpendicular component of the electric field, we can also observe the salient existence of the parallel electric field. It indicates that there exists a plasma density mode accompanying this Alfvén wave event. Here, the plasma beta is estimated to be $\beta_{||p} \approx 0.025$ following Equation (4) in Yue et al. (2016), which is very small; therefore, the conditions are similar to those in the solar corona.

The banded structure in this wave event is shown more clearly in Figure 2(a), which displays the spectrum of the perpendicular magnetic field as a function of frequency at 04:46:00 UT. The black arrows pointing at 0.39 Hz and 1.55 Hz denote f_{O^+} and f_{He^+}, respectively. The blue dashed line at $f_1 = 0.66$ Hz represents the peak frequency of the fundamental wave, while the red, gray, orange, magenta, and green dashed lines denote the frequencies f_1 at times $n = 2$, 3, 4, 5, and 6, respectively. It is evident that the spectrum consists of one fundamental wave and five/six harmonic waves. The highest harmonic wave has the frequency 4.5–5 Hz, which is about 0.75–0.83 of the proton gyrofrequency. In general, the amplitudes of the harmonic waves decrease with the increase of their frequencies, except for the third harmonic wave, which damps heavily. Cyclotron resonant absorption by He^+ could be a reason, and this will be discussed later.

The fundamental wave and its second harmonic wave have relatively high amplitudes (1–2 nT), while those of higher harmonics are weaker and less than 0.5 nT, as displayed in Figure 2(b). Unlike the fundamental wave, which has only one peak amplitude at about 04:48:10 UT, almost all the harmonics have double peaks in amplitude at about 04:45:40 UT and 04:48:10 UT. This is consistent with the double-peak structure in $E_{||}$ spectrum in Figure 1(d), suggesting the generation of the harmonics may be associated with the plasma density modes. Figures 2(c)–(e) clearly illustrate the waves are quasi-parallel ($\theta_{\rm avg} < 20^{\circ}$) and counter-propagating ($-1 < P_{\rm avg} < 1$), with nearly linear polarization ($\varepsilon_{\rm avg} \approx 0$).

We suggest that the harmonic waves are generated due to the coupling between the fundamental waves and the accompanied plasma density modes, which can be demonstrated by the corresponding bicoherence index. This index has been commonly used to measure the resonant coupling due to three-wave interactions (van Milligen et al. 1995; Soucek et al. 2003; Nariyuki & Hada 2006; Gao et al. 2016). Here, the waveform data of one arbitrary perpendicular component of the electric field δE_y and the parallel electric field δE_z for a 3 min interval from 04:44:00 UT are chosen to calculate the bicoherence index, leading to $bc = |\langle \delta E_z(f_{Ez})\delta E_y(f_{Ey})\delta E_y^*(f_{\rm HW})\rangle|^2 / \langle|\delta E_z(f_{Ez})\delta E_y(f_{Ey})|^2\rangle \langle|\delta E_y^*(f_{\rm HW})|^2\rangle$ (where the bracket $\langle\ldots\rangle$ denotes an average over the 3 min interval, and $f_{\rm HW} = f_{Ez} + f_{Ey}$ is the frequency of the wave generated due to the coupling between two pump waves). Note that the large bicoherence (close to 1.0) indicates the three wave modes satisfy the resonant conditions, i.e., $f_{\rm HW} = f_{Ez} + f_{Ey}$, and $\boldsymbol{k}_{\rm HW} = \boldsymbol{k}_{Ez} + \boldsymbol{k}_{Ey}$ (Lagoutte et al. 1989). We can easily find that the bicoherence indices become large at (mf_1, nf_1), where $f_1 = 0.66$ Hz is the frequency of the fundamental wave, m, n are nonzero integers, and $m + n = 2$, 3, 4, 5, and 6 (Figure 3). Note that the bicoherence index actually cannot provide the causal relation. However, we find that the amplitude of the fundamental Alfvén wave is larger than that of the higher harmonics (Figure 2(b)). Besides, Alfvén waves are found to be easily coupled with ion density modes in a low-beta plasma (Gao et al. 2013; He et al. 2016). Therefore, we propose that the higher harmonics are generated through the nonlinear coupling between the fundamental wave and the associated density fluctuations, which can be considered as the energy cascade of the fundamental Alfvén wave.

To obtain the wave number of each band wave, we utilize the Waves in Homogeneous Anisotropic Magnetized Plasma (WHAMP) model (https://github.com/irfu/whamp, Rönnmark 1983) to calculate the linear dispersion curves. Here, the plasma parameters are extracted from 04:43:30 UT, including the electron density $n_e = 45.9\,{\rm cm}^{-3}$, the magnetic field $B_0 = 430\,nT$, the proton gyrofrequency $f_{cp} = 6.6$ Hz, and the properties of the fundamental Alfvén waves: the wave normal angle $\theta = 10.69^{\circ}$ and frequency $f_1 = 0.66$ Hz (i.e., $f_1 = 0.1 f_{cp}$). We assume this plasma system only consists of cool protons and electrons with a Maxwellian velocity distribution, and they have the same temperature, $T_p = T_e = 27$ eV. Then, the wave number of the fundamental wave can be obtained to be $k_1 c/\omega_{pp} = 0.33$ (where c is the light speed and ω_{pp} is the proton plasma frequency). Based on the resonant conditions between the fundamental Alfvén wave and its harmonics, we can estimate the wave numbers of the harmonic wave modes to be $k_n = nk_1$. Also, the cyclotron resonant condition of wave–particle interactions is given by

$$2\pi f_n - k_{n||} v_{i||} = \pm 2\pi f_{ci}, \quad (1)$$

where i represents the particle species, H^+, He^+, O^+, $v_{i||}$ is the parallel velocity for different particle species i, and f_{ci} is the

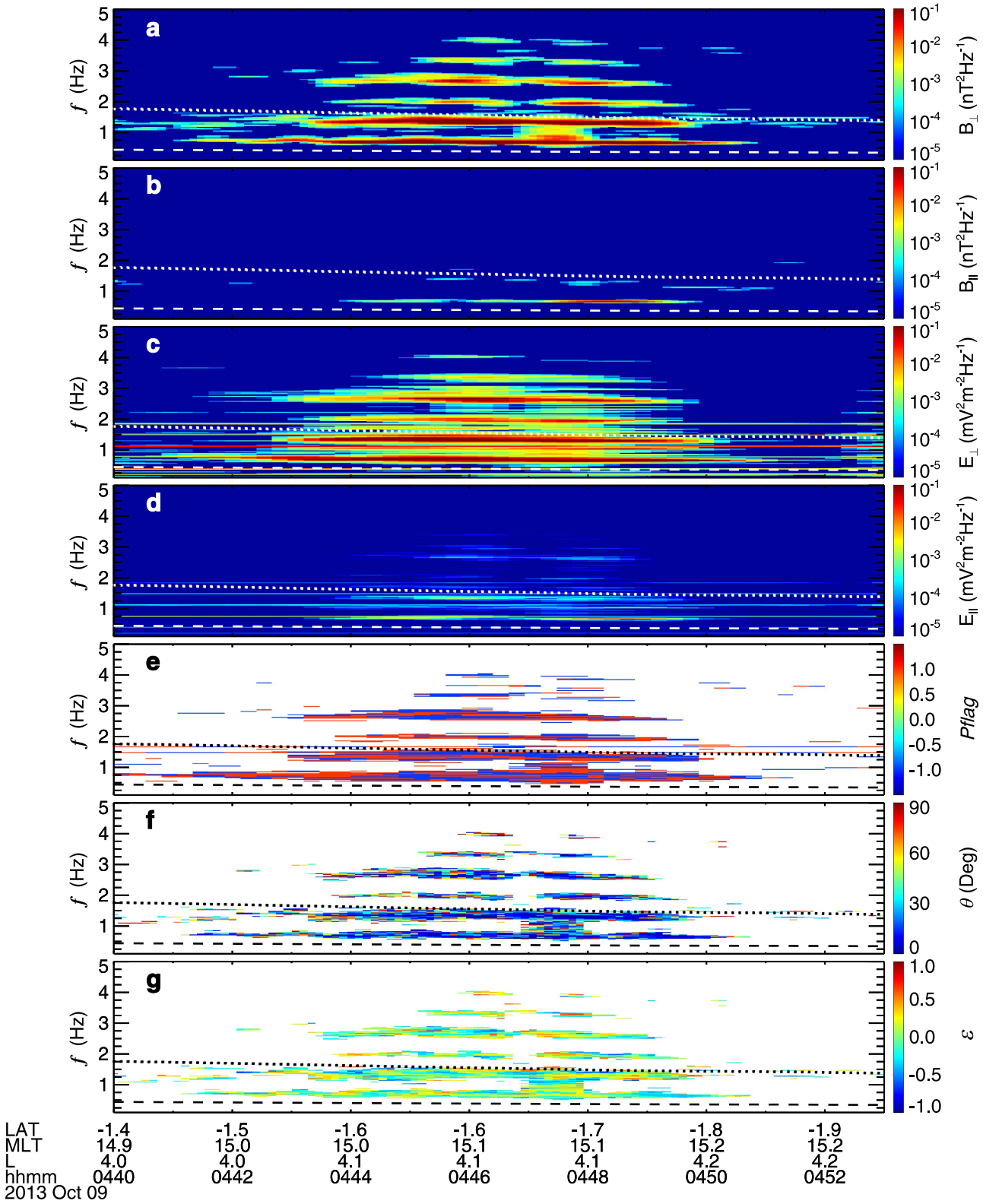

Figure 1. One harmonic Alfvén event observed by *Van Allen Probe* B on 2013 October 9 showing: (a)–(d) The dynamic spectrogram of fluctuating magnetic ($B_\perp$ and $B_{||}$) and electric ($E_\perp$ and $E_{||}$) fields, respectively, which are obtained by fast Fourier analysis; (e) a flag, i.e., "Pflag," representing the wave propagating direction; (f) the wave normal angle θ; and (g) the ellipticity ε. In all panels, the dotted and dashed lines in black or white represent the local helium gyrofrequency f_{He^+} and oxygen gyrofrequency f_{O^+} , respectively.

gyrofrequency for different particle species i. In the right-hand term of Equation (1), "+/−" is chosen when the waves have left-hand/right-hand polarization. In our observations, the waves have nearly linear-polarization, and a linear-polarized wave can be considered to the superposition of a left-hand and right-hand wave with the same frequency. Once we know the

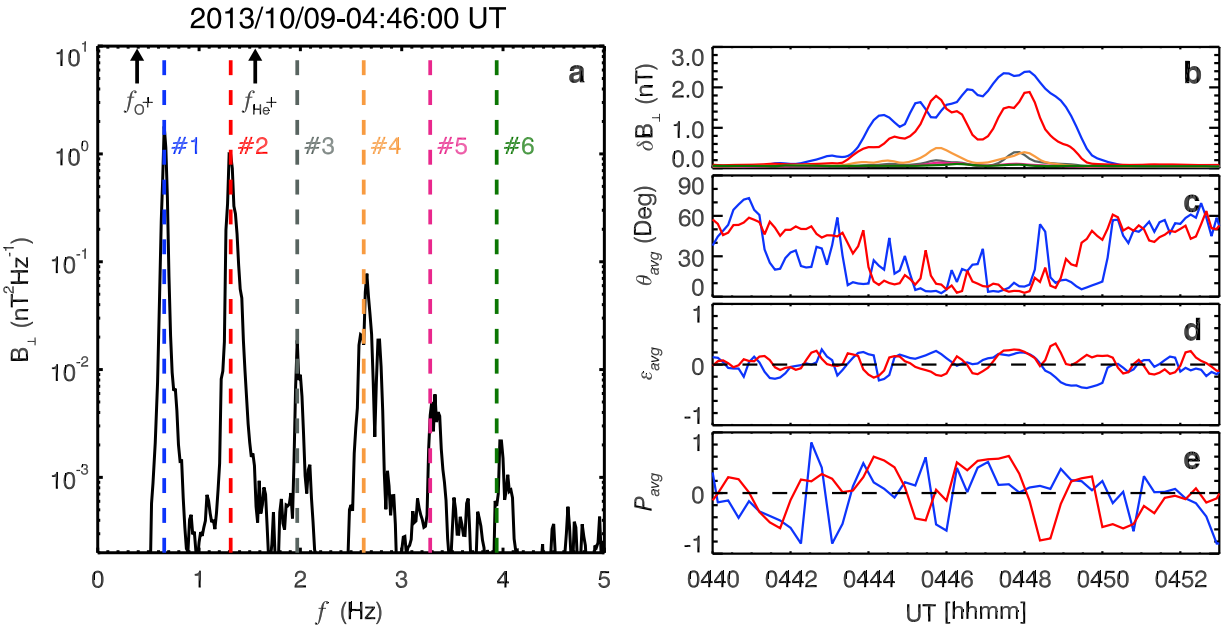

Figure 2. (a) Magnetic power as a function of frequency at 04:46:00 UT. The black arrows pointing at 0.39 Hz and 1.55 Hz denote f_{O^+} and f_{He^+}, respectively. The blue dashed line at $f_1 = 0.66$ Hz represents the peak frequency of fundamental wave, while the red, gray, orange, magenta, and green dashed lines denote the frequencies f_1 at times $n = 2$, 3, 4, 5 and 6, respectively. Also shown are the time evolutions of (b) the amplitude $\delta B_\perp$ in different wave bands, the averaged (c) wave normal angle θ_{avg}, (d) ellipticity ε_{avg}, and (e) Pflag P_{avg}, which are all power-weighted mean values over each band at every time segment. The black dashed line in Figures 2(d) and (e) represent $\varepsilon_{avg} = 0$ and $P_{avg} = 0$. Since the higher harmonics have low amplitude, we only perform the averaged properties of the fundamental wave (blue) and second harmonic wave (red) in panels (c)–(e).

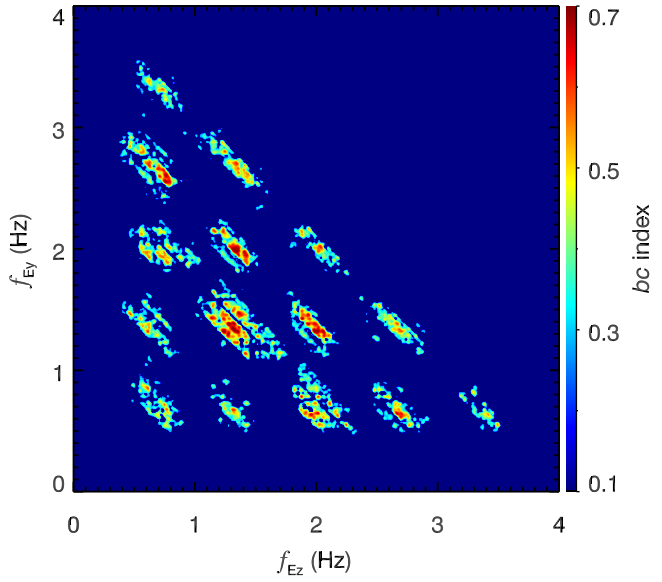

Figure 3. Distribution of bicoherence index in the $f_{Ez} - f_{Ey}$ domain for the time interval 04:44:00–04:47:00 UT, which is defined as $bc = |\langle \delta E_z(f_{Ez}) \delta E_y(f_{Ey}) \delta E_y^*(f_{HW}) \rangle|^2 / \langle |\delta E_z(f_{Ez}) \delta E_y(f_{Ey})|^2 \rangle \langle |\delta E_y^*(f_{HW})|^2 \rangle$. The large bicoherence index (close to 1) suggests the three wave modes satisfy the resonant condition, i.e., $f_{HW} = f_{Ez} + f_{Ey}$, and $\boldsymbol{k}_{HW} = \boldsymbol{k}_{Ez} + \boldsymbol{k}_{Ey}$ (Lagoutte et al. 1989).

frequencies and wave numbers of the waves, and gyrofrequencies of the different particles, we can calculate the resonant parallel velocities for the particles. Then, we can estimate the minimum resonant energies for different wave modes, as shown in the Table 1.

The H^+ differential flux as a function of pitch angle (PA) and universal time in four lower-energy (a) 0.8–44.4 keV and four higher-energy channels (b) 81.6–488.9 keV is illustrated in Figure 4. The fundamental Alfvén waves can cyclotron resonantly interact with the protons when the energy of the protons is larger than about 76.53 keV. From Figure 4(b), we see that in the energy channel 81.6 keV, the energetic proton flux around the PA around 90° tends to decrease, while the flux around PA around 0° and 180° increases. This is consistent with the results of Alfvén waves excited by the proton temperature anisotropy (Lu & Wang 2006). Therefore, the source energy of the observed fundamental Alfvén waves should be provided by energetic protons with energy above 76.53 keV. The harmonic waves can cyclotron resonantly scatter the protons with energy below 76.53 keV, where the energetic proton flux around the PA around 90° increases, clearly exhibited in Figure 4(a).

Moreover, we further present the PA distribution of (a) He^+ and (b) O^+ as a function of universal time for six different energy channels in Figure 5. The fundamental Alfvén waves and their harmonics can cyclotron resonantly interact with the heavy ions (such as He^+, O^+) with much lower energy (see Table 1) than that of protons. Note that the third harmonic can resonantly scatter He^+ ions even when their energy is very low (~0.11 keV), and this should be the reason that the amplitude of the third harmonic is even smaller than that of the fourth

Table 1
Minimum Resonant Energies of Different Wave Modes[a]

	I	II	III	IV	V	VI
$E_{H^+(m)}$ (keV)	76.53	15.10	5.13	2.12	0.94	0.42
$E_{He^+(m)}$ (keV)	8.47	0.23	0.11	0.54	0.96	1.30
$E_{O^+(m)}$ (keV)	2.17	7.23	9.57	10.86	11.68	12.24

Note.
[a] Selected time 2013/10/09-04:43:30 UT.

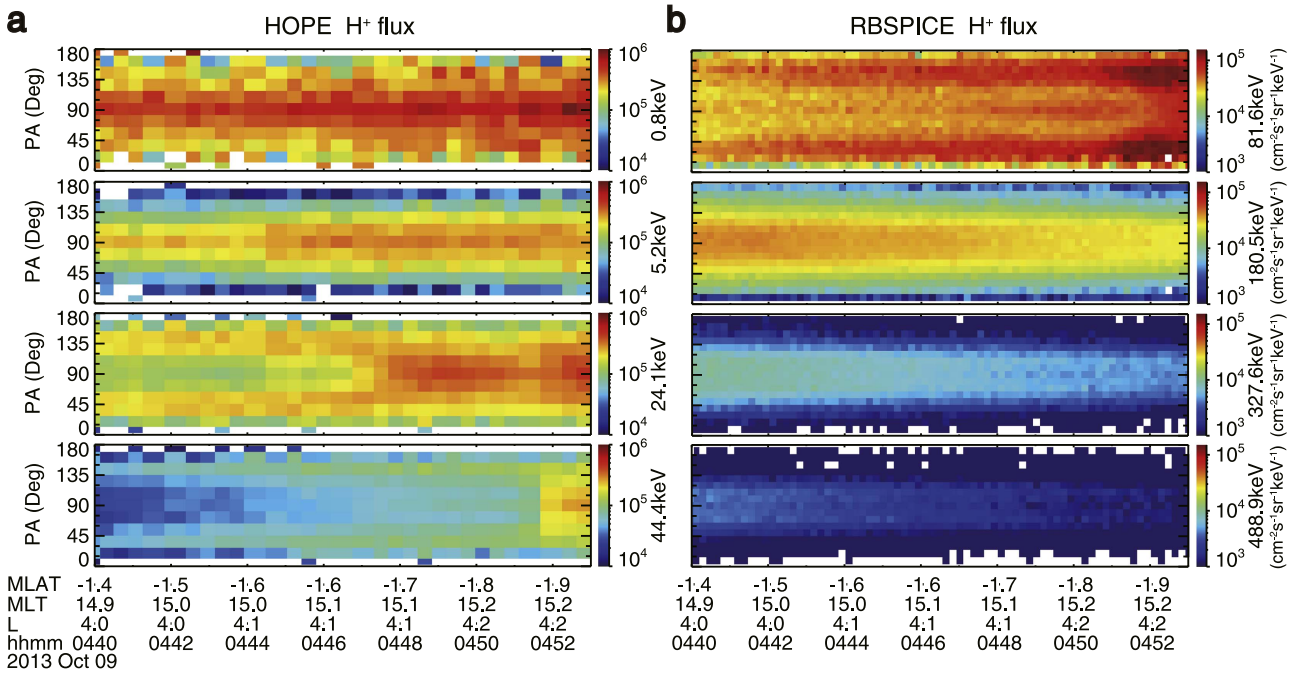

Figure 4. Pitch angle distributions of H^+ in four lower-energy channels (a) 0.8–44.4 keV measured by HOPE, and four higher-energy channels (b) 81.6–488.9 keV measured by RBSPICE as a function of universal time.

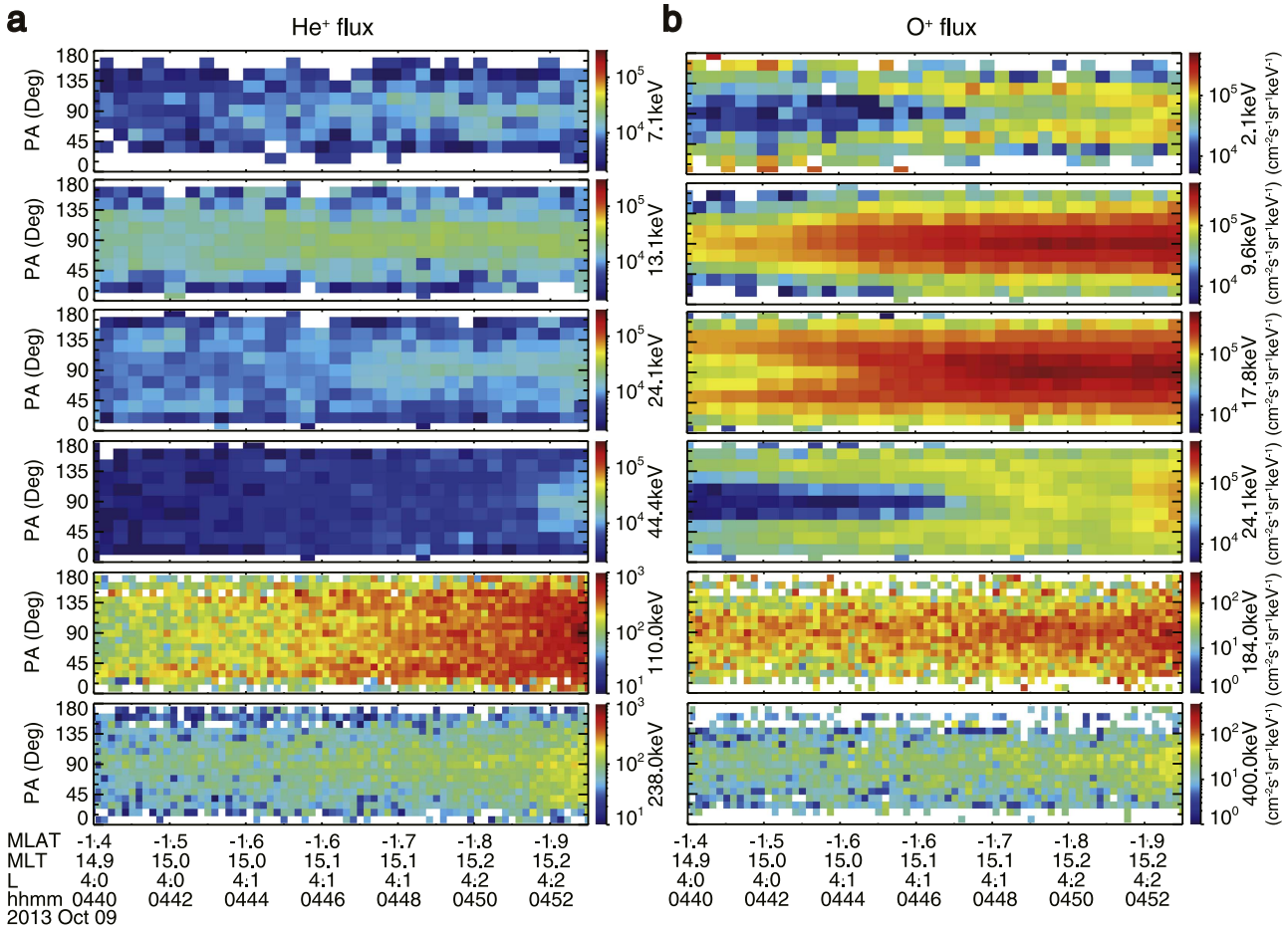

Figure 5. Pitch angle distributions of (a) He^+ and (b) O^+ as a function of universal time for six different energy channels. The top four panels are from HOPE, and the bottom two panels are from RBSPICE.

harmonic. Also, the flux of both He^+ and O^+ around the PA 90° increases at all levels of the measured energies (Figure 5), and it means that the waves can preferentially heat the heavy ions in the perpendicular direction. The results are similar to remote-sensing observations of the coronal hole in the solar corona (Kohl et al. 1997, 1998).

4. Conclusions and Discussion

In summary, we have presented an unusual harmonic Alfvén event on 2013 October 9 measured by the *Van Allen Probes* in the magnetosphere. In this event, we identify two quasi-parallel counter-propagating Alfvén waves (fundamental waves) with almost identical frequency, which are accompanied by a plasma density mode. The fundamental Alfvén waves could be excited by the anisotropic protons with energy greater than about 76.53 keV. Besides the fundamental Alfvén waves, several harmonic Alfvén waves, which propagate almost along the wave vector of the fundamental waves, are also identified in the observations. The bicoherence index demonstrates strong wave–wave coupling processes among the Alfvén waves, which may indicate an energy cascade from the fundamental to the harmonic Alfvén waves. The latter can modulate the ion PA distribution efficiently through cyclotron resonant interactions, and then preferentially heat heavy ions in the perpendicular direction.

In fact, the observed quasi-parallel propagating Alfvén waves with unexpected linear polarization are not rare events, and they have been reported in many previous works (Anderson et al. 1996; Meredith et al. 2003; Yu et al. 2015). However, there is still no consensus about their generation mechanism. They may be excited through some unknown nonlinear processes, or just due to the superposition between two constituent waves (Denton et al. 1996). This is also an interesting topic, but is beyond the scope of this paper and left to a future study.

Because the plasma environment here is similar to that of the solar corona, our observations can potentially shed light on the generation of the high-frequency Alfvén waves through cascade, which is obligatory for heating ions in the solar corona via cyclotron resonant scattering, and may be produced due to the coupling between the low-frequency Alfvén waves and the accompanied plasma density modes. These high-frequency waves will heat ions primarily in the perpendicular direction, which is consistent with remote-sensing observations of the solar corona (Kohl et al. 1997, 1998; Li et al. 1998; Cranmer et al. 1999). Moreover, the *Solar Probe Plus* mission, which is intended to present in situ observations of the low solar corona and determine the exact mechanism how the solar corona and wind are heated and accelerated (Fox et al. 2016), could provide a more comprehensive understanding of Alfvénic cascade. Therefore, our observations may provide a new insight into ion heating in the solar corona.

This research was supported by the NSFC grant 41604128, 41631071, 41331067, 41474125, Youth Innovation Promotion Association of Chinese Academy of Sciences (No. 2016395), and Key Research Program of Frontier Sciences, CAS (QYZDJ-SSW-DQC010). We also acknowledge the entire *Van Allen Probes* instrument team and the *Van Allen Probes* data used here, obtained from https://spdf.sci.gsfc.nasa.gov/pub/data/rbsp/rbspb.

ORCID iDs

Huayue Chen https://orcid.org/0000-0002-7619-701X
Xinliang Gao https://orcid.org/0000-0003-0767-2267
Quanming Lu https://orcid.org/0000-0003-3041-2682

References

Anderson, B. J., Denton, R. E., & Fuselier, S. A. 1996, JGR, 101, 13195
Bale, S. D., Kellogg, P. J., Mozer, F. S., Horbury, T. S., & Reme, H. 2005, PhRvL, 94, 215002
Bortnik, J., Cutler, J. W., Dunson, C., & Bleier, T. E. 2007, JGR, 112, A4204
Cranmer, S. R. 2000, ApJ, 532, 1197
Cranmer, S. R., Field, G. B., & Kohl, J. L. 1999, ApJ, 518, 937
Cranmer, S. R., & van Ballegooijen, A. A. 2003, ApJ, 594, 573
Denton, R. E., Anderson, B. J., George, Ho., & Hamiton, D. C. 1996, JGR, 101, 24869
Fox, N. J., Velli, M. C., Bale, S. D., et al. 2016, SSRv, 204, 7
Funsten, H. O., Skoug, R. M., Guthrie, A. A., et al. 2013, SSRv, 179, 423
Gao, X. L., Lu, Q. M., Bortnik, J., et al. 2016, GeoRL, 43, 2343
Gao, X. L., Lu, Q. M., Li, X., Shan, L. C., & Wang, S. 2013, PhPl, 20, 072902
Gary, S. P., & Nishimura, K. 2004, JGR, 109, A02109
Goldreich, P., & Sridhar, S. 1995, ApJ, 438, 763
He, J. S., Tu, C. Y., Marsch, E., & Yao, S. 2012, ApJL, 745, L8
He, P., Gao, X. L., Lu, Q. M., & Wang, S. 2016, ApJ, 827, 64
Hollweg, J. V. 1999, JGR, 104, 24781
Hollweg, J. V., & Johnson, W. 1988, JGR, 93, 9547
Howes, G. G., Cowley, S. C., Dorland, W., et al. 2008, JGR, 113, A05103
Isenberg, P. A., & Hollweg, J. V. 1983, JGR, 88, 3923
Isenberg, P. A., Lee, M. A., & Hollweg, J. V. 2001, JGR, 106, 5649
Kessel, R. L., Fox, N. J., & Weiss, M. 2012, SSRv, 179, 531
Kletzing, C. A., Kurth, W. S., Acuna, M., et al. 2013, SSRv, 179, 127
Kohl, J. L., Noci, G., Antonucci, E., et al. 1997, SoPh, 175, 613
Kohl, J. L., Noci, G., Antonucci, E., et al. 1998, ApJL, 501, L127
Lagoutte, D. F., Lefeuvre, F., & Hanasz, J. 1989, JGR, 94, 435
Leamon, R. J., Smith, C. W., Ness, N. F., & Wong, H. K. 1999, JGR, 104, 22331
Li, X., Habbal, S. R., Kohl, J. L., & Noci, G. 1998, ApJL, 501, L133
Lu, Q. M., & Wang, S. 2006, JGR, 111, A05204
Mauk, B. H., Fox, N. J., Kanekal, S. G., et al. 2013, SSRv, 179, 3
Meredith, N. P., Throne, R. M., Horne, R. B., et al. 2003, JGR, 108, 1250
Mitchell, D. G., Lanzerotti, L. J., Kim, C. K., et al. 2013, SSRv, 179, 263
Nariyuki, Y., & Hada, T. 2006, NPGeo, 13, 425
Podesta, J. H., & TenBarge, J. M. 2012, JGR, 117, A10106
Quataert, E. 1998, ApJ, 500, 978
Rönnmark, K. 1983, PhPl, 25, 669
Sahraoui, F., Goldstein, M. L., Belmont, G., & Reaeau, L. 2010, PhRvL, 105, 131101
Santolik, O., Pickett, J. S., Gurnett, D. A., et al. 2010, JGR, 115, A00F13
Soucek, J., Dudok de Wit, T., Krasnoselskikh, V., & Volokitin, A. 2003, AnGeo, 21, 681
Sridhar, S., & Goldreich, P. 1994, ApJ, 432, 612
Tu, C. Y. 1987, SoPh, 109, 149
Tu, C. Y., & Marsch, E. 1997, SoPh, 171, 363
Usanova, M. E., Malaspina, D. M., Jaynes, A. N., et al. 2016, GeoRL, 43, 8827
van Milligen, B. P., Sanchez, E., Estrada, T., et al. 1995, PhPl, 2, 3017
Vasquez, B. J., Markovskii, S. A., & Chandran, B. D. G. 2014, ApJ, 788, 178
Wygant, J. R., Bonnell, J. W., Goetz, K., et al. 2013, SSRv, 179, 183
Yu, X. D., Yuan, Z. G., Wang, D. D., et al. 2015, GeoRL, 42, 1312
Yue, C., An, X., Bortinik, J., et al. 2016, GeoRL, 43, 7804